Electronic Theses and Dissertations

Student Works

8-2019

Electrodeposition of Hydrogen Molybdenum Bronze Films and Electrochemical Reduction of Carbon Dioxide at Low Over Potentials

Sami Alharbi
East Tennessee State University

Follow this and additional works at: https://dc.etsu.edu/etd

 Part of the Analytical Chemistry Commons, and the Oil, Gas, and Energy Commons

Electrodeposition of Hydrogen Molybdenum Bronze Films and Electrochemical Reduction of

Carbon Dioxide at Low Over Potentials

_____

A thesis

presented to

the faculty of the Department of Chemistry

East Tennessee State University

In partial fulfillment

of the requirements for the degree

Master of Science in Chemistry

_____

by

Sami Alharbi

August 2019

_____

Dr. Dane W. Scott, Chair

Dr. Greg Bishop

Dr. Catherine McCusker

Keywords: Electrodeposition, Reduction of Carbon Dioxide, Formate, Ion chromatography

ABSTRACT

Electrodeposition of Hydrogen Molybdenum Bronze Films and Electrochemical Reduction of

Carbon Dioxide at Low Over Potentials

by

Sami Alharbi

Hydrogen molybdenum oxide, known has molybdenum bronze, is a material of interest due to

catalyzing electron transfer reactions. Specifically, molybdenum bronze is an electrocatalyst

toward carbon dioxide reduction. Electrochemical deposition from a peroxymolybdic acid

solution is a method for preparing molybdenum bronze films. This work demonstrates

reproducible electrodeposition on indium tin oxide substrates and conductive carbon paper. Film

thickness depends on concentration, time and pH. After characterization by film thickness,

resistance, XRD and XPS, the as deposited films served as the working electrode for

electrochemical reduction of carbon dioxide in 0.1 M $NaHCO_3$. Ion chromatography determined

formate resulting in 8% faradaic efficiency at an applied potential of -0.4 V. Interestingly, this

potential is similar to use of formate dehydrogenase as an electrocatalyst. Carbon monoxide

levels were attempted to be determined by GC in the headspace of an H type electrochemical

cell. Results show that these films are applicable towards electrochemical CO_2 reduction to

formate when supported on carbon.

DEDICATION

This work is dedicated to my family: my parents, and my friend who have supported me along my journey.

ACKNOWLEDGEMENTS

TABLE OF CONTENTS

6

LIST OF TABLES

LIST OF FIGURES

LIST OF ABBREVIATIONS

CV   Cyclic voltammetry

CVD   Chemical vapor deposition

FDH   Formate dehydrogenase

FE   Faradaic efficiency

GCP   Global carbon project

ITO   Indium tin oxide

NHE   Normal hydrogen electrode

NP   Nanoporous

RHE   Reversible hydrogen electrode

SHE   Standard Hydrogen Electrode

XPS   X-ray photoelectron spectroscopy

XRD   X-ray diffraction

CHAPTER 1

INTRODUCTION AND PURPOSE OF RESEARCH

Research efforts have been focused on reduction of carbon dioxide both photochemically and electrochemically. One known problem in electrochemical reduction of carbon dioxide (CO_2) is poisoning of metal catalysts by carbon monoxide (CO) on carbon supports.[1] Recently, hydrogen molybdenum bronze films have been used as a catalytic support for platinum for oxidation of methanol. The hydrogen molybdenum bronze was shown to prevent CO poisoning of platinum.[2] A hydrogen bronze is normally molybdenum (Mo), vanadium (V) or tungsten (W) oxide with hydrogen intercalated in the solid matrix. Bronzes can be prepared by a variety of methods. For example, chemical vapor deposition (CVD) followed by oxidation or electrodeposition results in molybdenum oxide (MoO_3) films.[3-10] The formula of the hydrogen bronze is H_xMoO_3, where x is between 0.46 and 1.63.[11-13] Interestingly, hydrogen intercalation into the oxide matrix is electrochemically reversible. These films are blue with hydrogen and colorless when hydrogen is removed.   Importantly, hydrogen bronze films have a high surface area and are excellent for catalyzing reactions involving transfer of electrons.[12] An example of this is hydrogen molybdenum bronze used as an electron donor for the reduction of p-nitrophenol to p-aminophenol.[14] This property serves as the rational for exploring hydrogen molybdenum bronze films as a catalyst supported on carbon for reduction of CO_2. The main goals are to lower the required overpotential and possibly reduce the effect of CO poisoning of the catalyst. Thus, research work presented explores electrodeposition of hydrogen molybdenum bronze films on carbon for electrochemical reduction of CO_2 to formate.

Hydrogen Bronze Materials

A hydrogen bronze is a metal oxide film that has hydrogen present in the oxide matrix. For example, hydrogen molybdenum bronze has the formula $H_x Mo_x^{5+} Mo_{1-x}^{6+} O_3$.[15] Tungsten and vanadium oxide are also examples of metals that form bronzes. These films are important because of exciting electromechanical properties and explored as chemical sensors, for neutralization of explosives, chemical catalysis as electron donors and use in solar cells.[10,16-19] A hydrogen bronze may be prepared through a variety of strategies. These include metal vapor deposition followed by oxidation, sol-gel strategies, thermal decomposition of ammonium heptamolybdate or reacting the oxide with alcohols or glycols.[3, 20-23] Hydrogen ions when intercalated into molybdenum oxide films form what is known as hydrogen bronze. Hydrogen intercalation was studied using a hydrogen molybdenum bronze powder pressed as a pellet with one side exposed to sulfuric acid and silver paste on the other side. The sample was studied by cyclic voltammetry (CV) in dilute sulfuric acid showing reversible intercalation of hydronium ions into the molybdenum oxide lattice.[24] Hydrogen bronze films may also be prepared as a film using electrochemical deposition. The bronze film maybe deposited on metal substrates or indium tin oxide (ITO).[24] Two essential techniques include either dissolution of molybdenum metal or powder in hydrogen peroxide making peroxymolybdic acid which also serves as the electrolyte for electrodeposition or dissolving sodium molybdate and adding hydrogen peroxide.[7, 16, 25-28] The mechanism of electrodeposition is not fully understood.[29] Adding hydrogen peroxide to molybdate forms peroxymolybdate shown in Equation (1).[29]

$$[MoO_4]^{2-} + 2\ H_2O_2 \rightleftharpoons [MoO_2(O_2)_2]^{2-} + 2\ H_2O \quad (1)$$

The solution forms a yellow color which disappears over time due to the amount of hydrogen peroxide decreasing over time.[29] This work found that adding additional peroxide after adjusting

to a pH of 2.0 using sulfuric acid with additional peroxide resulted in stable peroxymolybdic acid shown in Equation (2), which is yellow.[29]

$$H^+ + [MoO_2(O_2)_2]^{2-} \rightleftharpoons [HMoO_2(O_2)_2]^{2-} \quad (2)$$
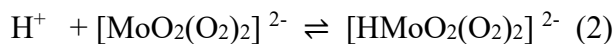
This research investigates the electrodeposition of peroxymolybdic acid onto indium tin oxide (ITO) coated glass slides and carbon paper. The films were utilized for reduction of CO_2. Carbon dioxide and reduction strategies are discussed below.

Carbon Dioxide

The carbon cycle is the way nature reuses carbon. Plants utilize sunlight and carbon dioxide for making sugar and release oxygen as shown in Equation (3).[30]

$$6\ CO_2 + 6\ H_2O + \text{Light energy} \rightarrow C_6H_{12}O_6 + 6O_2 \quad (3)$$
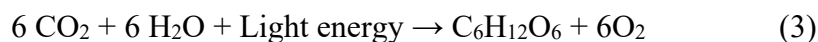
Carbon returns to the atmosphere by decay of plants, animals, as well as through the process of respiration. Dead plants that are buried turn into carbon based oils and fossil fuels over thousands of decades. Burning of fossil fuels results in adding this carbon back into the atmosphere.[30] Also, Oceans absorb carbon dioxide and the increasing uptake of carbon dioxide decreases the pH of the ocean resulting in ocean acidification due to the formation of carbonic acid. Over the last two centuries, oceans have absorbed more than 500 billion tons of carbon dioxide causing a 30% increase of carbon levels in the oceans.[30] Carbon dioxide also naturally comes from the decomposition of organic matter by soil-dwelling organisms such as bacteria and fungi.[31] Phytoplankton play critical role in regulating carbon cycle consuming carbon dioxide. When phytoplankton die, they sink to the bottom of the ocean, decompose and convert to organic matter resulting in dissolved carbon dioxide.[31] Furthermore, a significant amount of carbon dioxide is also released during the process of respiration carried out by living organisms.[32,33]

This reaction is very important in all living organisms to produce energy and is shown in Equation (4).

$$C_6H_{12}O_6 + 6O_2 \rightarrow 6CO_2 + 6H_2O + \text{Energy} \quad (4)$$
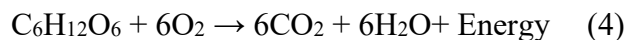
These processes and human activity have resulted in an increase in CO_2 levels in the atmosphere overtime. The average carbon dioxide emissions reported by the Global Carbon Project (GCP) was 37.1 billion tons during 2018.[34] The GCP report suggests that carbon dioxide emissions increased by 2.7% in year 2018 compared to the previous year 2017, during which there was a 1.6% increase.[35] According to the data presented by Statista, the global carbon dioxide emissions are expected to rise from 33.9 to 34.97 billion metric tons in the year 2019-2020.[36]
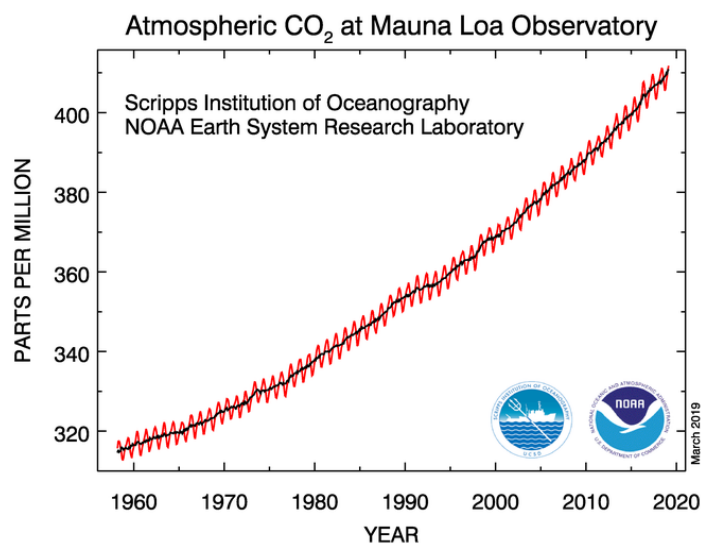
Figure 1. Atmospheric CO_2 levels and year as measured by the Earth System Research Laboratory. Reprinted by permission from NOAA/ESRL Global Monitoring Division

The amount of atmospheric CO_2 in ppm and year is shown in Figure 1 obtained from the National Oceanic and Atmospheric Administration's Earth System Research Laboratory website.[37] Many research groups are currently working on advanced technological interventions

that can convert carbon dioxide into useful products thus reducing CO_2 levels. There is

significant interest in reduction of carbon dioxide to methane and formate, which are feedstocks

for fuel cell technology.[37]

<div align="center">Reduction of CO2 for Use in Fuel Cells</div>

Methane and formate may also be used in the fuel cells to generate electricity. In direct

methane fuel cells, platinum is used as a catalyst to facilitate oxidation of methane to generate

electricity.[38] The individual half reactions, overall reaction and potentials with respect to the

standard hydrogen electrode (SHE) for the methane fuel cell are given in Equations 5-7.[38,39,40]

Anode: $CO_2(g) + 8H^+ + 8e^- \rightleftharpoons CH_4(g) + 2\ H_2O$ $E° = +0.169\ V$ (5)

Cathode: $O_2(g) + 4H^+ + 4e^- \rightleftharpoons 2\ H_2O$ $E° = +1.23\ V$ (6)

Overall: $CH_4 + 2O_2 \rightleftharpoons CO_2 + 2H_2O$ $E° = +1.06\ V$ (7)
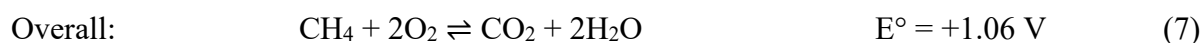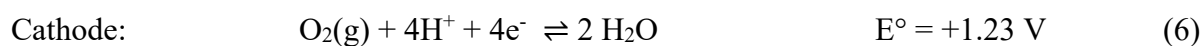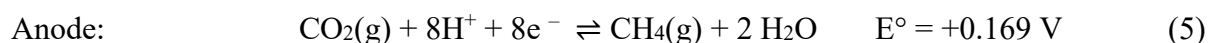
As an example, a methane fuel cell operating at 80° C provided 403 µW/mg using platinum(II)

bipyridine complexes.[38]

A formate fuel cell has the advantage of operating at lower temperatures compared to

methane fuel cells and operate at standard temperature and pressure.[41] The half cell reactions,

potentials vs. the SHE and overall reaction for an air and formate fuel cell are given in Equations

8-10.

Anode: $CO_3^{2-} + 2\ H_2O + 2\ e^- \rightleftharpoons HCOO^- + 3\ OH^-$ $E° = -1.05\ V$ (8)

Cathode: $½\ O_2 + H_2O + 2\ e^- \rightleftharpoons 2\ OH^-$ $E° = +0.4\ V$ (9)

Overall: $HCOO^- + ½\ O_2 + OH^- \rightleftharpoons CO_3^{2-} + H_2O$ $E° = +1.45\ V$ (10)
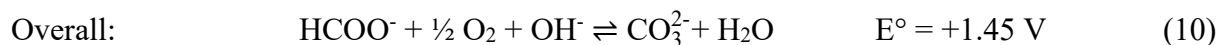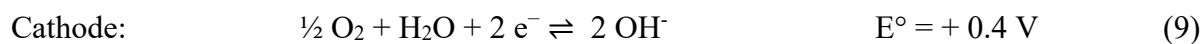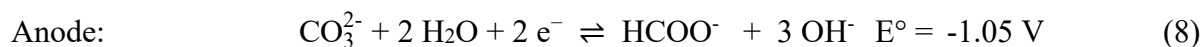
With the cathode on the right and hydroxide ions moving toward the anode on the left this results

in an overall theoretical potential of +1.45 V.[41] A recent example of a formate fuel cell resulted

in power density of 591 mW/cm^2 at 60 °C.[42] Basic conditions for fuel cell operation are preferred as under acidic conditions oxidation results in CO which passivates or poisons the catalytic metal surface.[42] The output power of formate fuel cells is typically less than 50 W.[42] One extensive area of research is reduction of CO_2 to value added compounds that can be used as a feedstock for fuel cells. Reduction methods include photocatalytic and electrochemical reduction. Carbon dioxide must be reduced efficiently to useful products to be realized as a feedstock for methane and formate fuel cells. Reduction of CO_2 to formate may be accomplished by either photochemical and/or electrochemical reduction.   Electrochemical reduction of CO_2 is reviewed.

<div align="center">Metal Electrodes for Electrochemical Reduction of Carbon Dioxide</div>

Several metals have been used as electrodes for electrochemical reduction of CO_2. Indium, tin, mercury and lead are selective for formic acid formation, while zinc, gold and silver favor carbon monoxide production, and copper favors formation of alcohols and hydrocarbons.[43] In a research study by Kaneco and co-workers, the electrochemical reduction of carbon dioxide at a copper electrode in methanol was investigated with various supporting electrolytes.[44] The findings of the study reported that the highest faradic efficiency was 70.5% using a NaClO$_4$/methanol-based electrolyte. When higher reduction potentials are used, byproducts such as ethane and methanol result.[44] At these high overpotentials a carbon monoxide is produced which inhibits catalytic activity. Another study investigated the conversion of carbon dioxide to methane at the copper electrode in the presence of methanol. The solution was enhanced with salt compounds at temperatures of 243 K. The reaction was successful in yielding carbon monoxide, methane and formic acid. This work was selective for electrochemical reduction of CO_2 to methane.[44]

Tin used as an electrode was investigated for formate production. The study showed that

tin served as an effective catalyst for production of formate, hydrogen and carbon monoxide.[45]

In all potentials the FE was observed to range between 90% and 100%. Hydrogen and formate

were initially detected at -0.44V versus the reversible hydrogen electrode (RHE) whereas carbon

monoxide was observed at -0.59 V.[45] Formate was the major product at -0.8V and reached a

maximum FE of 70% between -0.9 and -1.0 V whereas the maximum FE for CO was 17% at the

potential of -0.76 V. Through protonation the carbonate anion forms the formate ion which

desorbs into the electrolyte. The electrochemical reduction of CO_2 is dependent on the potential

applied, the transport of carbon dioxide and the metal used in the cathode. Tin, mercury, lead or

indium result in formate with faradaic efficiencies of 80% to 100%.[45] These metals are

established to have high hydrogen overpotentials reducing the amount of hydrogen gas

generated. Tin has been favored of the four metals in carbon dioxide reduction.[45] In addition,

significant work has been done using carbon supported catalysts for electrochemical reduction of

CO_2.
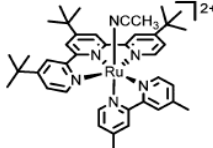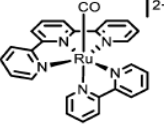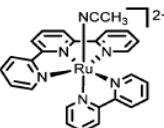
<p align="center">Electrocatalysts for Reduction of Carbon Dioxide</p>

The standard reduction potential of CO_2 to formate is -0.20 vs the RHE and is pH

dependent. The pH dependence is expressed by the equation (-0.2 + 0.059[pH-4]), when pH is

greater than 4.[46] Carbon dioxide has also been reduced electrochemically to several other

products using electroactive catalysts. For instance, electrochemical alloying of polycrystalline

gold with zinc using ethylene glycol and 1.5 M $ZnCl_2$ followed by dealloying using heat and

sulfuric acid can result in a 3D nanoporous structure for efficient electrochemical reduction of

carbon dioxide to carbon monoxide.[47] According to the results obtained, dealloyed gold had

current density over 65 times higher compared to the polycrystalline gold surface and three times

higher than the gold-zinc alloy at -0.6 V vs. RHE in a CO_2 saturated solution of 0.1 M

$NaHCO_3$.[47] The Faradaic efficiency (FE) of dealloyed gold at the applied potential of -0.6 V for

10 hours was high (95.9%).[47] This is an indication that surface structure plays a critical role in

electrochemical reduction of carbon dioxide to carbon monoxide.

In a similar experiment gold was functionalized with different thiol-tethered ligands for

electrochemical reduction of CO_2.[48] These thiol-tethered ligands included 2-mercaptopropionic

acid, cysteamine and 4-pyridinylethanemercaptan. In comparison to the gold foil, a 2 fold

increase in FE and 3 fold increase in the amount of formate produced was observed when 4-

pyridinylethanemercaptan was used. In addition, the use of 2- mercaptopropionic acid ligands

resulted in a FE of close to 100% for evolution of hydrogen. On the other hand, a 2-fold increase

in the production of both hydrogen gas and carbon monoxide was observed when a cysteamine

modified electrode was used.[48] Other studies that have been conducted in the bid to carry out

selective reduction of carbon dioxide to formate using metal electrodes.[49] Reduction of carbon

dioxide on a copper electrode resulted in the formation of a thick film of copper (II) oxide.[50]

Also, formate is a reduction product when using boron doped palladium catalysts.[51] Ruthenium

complexes are also well known electroactive catalysts for reduction of CO_2 resulting in Faradaic

efficiencies from 8 to 90% for formate.[52] Table 1 is a list of ruthenium complexes, conditions

and Faradaic efficiencies for comparative purposes. Carbon has been used as a support for

electrocatalytic reduction of CO_2.

Table 1. Ruthenium complexes for electrochemical reduction of CO_2. Reproduced from reference 52 by permission of The Royal Society of Chemistry

Entry	Molecule	Solvent	Applied potential[a]	Proton source[b]	Time (h)	Products (faradaic yields in %)	Ref.
1	$[Ru(bpy)_2(CO)_2]^{2+}$	H_2O/DMF (1:1)	−1.5 V vs. SCE	—	c	CO (51); H_2 (—); HCO_2^- (35)	63
2		H_2O/DMF (9:1) pH 6	−1.66 V	—	c	CO (27); H_2 (35)	63
3		H_2O pH 6	−1.66 V	—	c	CO (17); H_2 (54)	63
4		H_2O/DMF (1:1) pH 6	−1.5 V vs. SCE	—	c	CO (42); H_2 (3)	63
5		H_2O/DMF (9:1) pH 9.5	−1.66 V	—	c	CO (26); H_2 (37); HCO_2^- (38)	63
6	$[Ru(bpy)_2(CO)Cl]^{2+}$	H_2O/DMF (1:1)	−1.5 V vs. SCE	—	d	CO (55); H_2 (5); HCO_2^- (17)	63
7		H_2O/DMF (9:1) pH 6	−1.66 V	—	c	CO (21); H_2 (42);	63
8		H_2O/DMF (9:1) pH 9.5	−1.66 V	—	e	CO (28); H_2 (44); HCO_2^- (26)	63
9		CH_3CN	−1.68 V	0.2 M $MeNH_2$·HCl	c	HCO_2^- (64); CO (20); H_2 (3)	62
10		CH_3CN	−1.68 V	0.2 M Me_2NH·HCl	c	HCO_2^- (84); CO (2); H_2 (7)	62
11		CH_3CN	−1.68 V	0.2 M Me_3N·HCl	c	HCO_2^- (56); CO (6); H_2 (31)	62
12		CH_3CN	−1.68 V	$PhCO_2H$	c	HCO_2^- (23); CO (10); H_2 (51)	62
13		CH_3CN	−1.68 V	PhOH	c	HCO_2^- (81); CO (16); H_2 (<1)	62
14	cis-$[Ru(bpy)_2(CO)H]^+$	CH_3CN	−1.68 to −1.98 V	H_2O 3 mM to 0.40 M	f	CO (57); H_2 (8); HCO_2^- (17)	64
15[g]	trans(Cl)–$Ru(Mesbpy)(CO)_2Cl_2$	CH_3CN	−1.7 V	Phenol 0.5 M	h	CO (63); H_2 (2); HCO_2^- ([h])	65
16[g]		CH_3CN	−2.2 V	Phenol 0.5 M	h	CO (95); H_2 (1)	65
17	$Ru(tpy)(CO)(Cl)_2$	CH_3CN	−1.64 V	H_2O 20%	i	CO (60); HCO_2^- (10)	66
18		CH_3CN	−1.82 V	—	1	CO (95)	67
19[j]	$[Ru(tpy)(6DHBP)(S)]^{2+}$	CH_3CN	−2.3 V	—	1	CO (6); HCO_2^- (9)	68
20[k]	$[Ru(tpy)(4DHBP)(S)]^{2+}$	CH_3CN	−2.3 V	—	1	CO (14); HCO_2^- (18)	68
21		DMF/H_2O (2:8) pH 9	−1.70 V vs. Ag^+|Ag	—	h	CO (35); HCO_2H (30); H_2 (20); CH_3OH (0.4)	69
22		EtOH	−1.70 V vs. Ag^+|Ag	H_2O 20%	h	CO ([h]); HCO_2H ([h]); H_2 ([h]); CH_3OH (0.3)	69
23		EtOH	−1.70 V vs. Ag^+|Ag	H_2O 20%	c	HCHO ([h]); HCO_2H ([h]); H(O)COOH ([h]); $HOCH_2COOH$ ([h]); CH_3OH ([h]); CO ([h]);	69
24		CH_3CN	−2.3 V	—	1	CO (30); HCO_2^- (8)	68
25		CH_3CN	−2.21 V	—	5	CO (76); HCO_2^- (<20%); HCO_3^- ([h]); CO_3^{2-} ([h])	70
26		CH_3CN	−1.99 V	H_2O 10%	3	CO (90); H_2 (<2)	71
27		CH_3CN	−1.99 V	H_2O 10% H_3PO_4 50 mM	3	CO (43); H_2 (52)	71
28		CH_3CN	−1.99 V	H_2O 10% H_3PO_4 0.25 M	3	CO (35); H_2 (65)	71
29[l]	$[Ru(tpy)(Mebim-py)(S)]^{2+}$	CH_3CN	−2.15 V	—	5	HCO_3^- ([h]); CO_3^{2-} ([h]); CO (85); HCO_2^- (<20)	70
30[l]		CH_3CN	−2.14 V	H_2O 5%	3	CO (85); H_2 (<2); CH_3OH (—); HCHO (—); HCO_2^- (—)	72
31[m]	$[(bpy)_2Ru(dmbbbpy)]^{2+}$	CH_3CN	−2.08 V	H_2O 2%	d	HCO_2^- (89); CO (2–3)	73
32[m]		CH_3CN	−2.08 V	—	n	$C_2O_4^{2-}$ (64); CO (—); HCO_2^- (—)	73
33[m]	$[(bpy)_2Ru(dmbbbpy)Ru(bpy)_2]^{4+}$	CH_3CN	−1.98 V	H_2O 2%	h	HCO_2^- (90)	73
34[m]		CH_3CN	−1.98 V	—	h	$C_2O_4^{2-}$ (70)	73

[a] Potentials in V vs. Fc^+/Fc except otherwise noted. [b] % given by volume. [c] After 100 C passed. [d] After 90 C. [e] After 75 C. [f] After 4.8 to 28.2 C. [g] Mesbpy = 6,6′-dimesityl-2,2′-bipyridine. [h] Not specified. [i] After 68 C. [j] 6DHBP = 6,6′-dihydroxy-2,2′-bipyridine. [k] 4DHBP = 4,4′-dihydroxy-2,2′-bipyridine. [l] Mebim-py = 3-methyl-1-pyridylbenzimidazol-2-ylidene. [m] dmbbbpy = 2,2′-bis(1-methylbenzimidazol-2-yl)-4,4′-bipyridine, S = solvent. [n] After 50 C.

Carbon Supported Metal Catalysts for Electrochemical Reduction of CO_2

Carbon supports for electrochemical reduction of CO_2 is of interest because of having the capacity to covalently load metal and metalorganic catalysts. The effect is to improve faradaic efficiency.[40] For example, palladium incorporated into a carbon ink on titanium foil has been shown to carry out electrochemical reduction of CO_2. In 0.5 M $NaHCO_3$ saturated with CO_2 the FE diminishes by 80% at -0.35 V after three hours because of carbon monoxide poisoning.[53] Palladium nanoparticles drop dried on carbon support is another example in which faradaic efficiency for reduction of CO_2 is 97%. After an hour the FE drops rapidly because of catalytic poisoning.[54] Just last year, sulfur doped copper catalysts on carbon maintained a faradaic efficiency of up to 80% for over 12 hours. However, an over potential of -0.8 V vs. the Normal Hydrogen Electrode (NHE) was necessary.[55] Iron, nickel and cobalt nitrogen doped carbon electrocatalyts carried out reduction of CO_2 to CO with a FE of 93% demanding an over potential of 0.560 V. However, the FE decreases over the first two hours and held 63% percent efficiency following 12 hours.[56] Carbon supported metal alloys have also been used for CO_2 reduction.

Carbon Supported Metal Alloys for Electrochemical Reduction of CO_2

In a 2016 study, a tin-lead alloy on a carbon support was used as the electrocatalyst.[57] The electrochemical impedance spectroscopy measurements of the combined alloy exhibited a lower charge-transfer resistance value compared to the use of single metal electrodes.[57] The CV and X-ray Photoelectron Spectroscopy (XPS), on the other hand, showed that the tin present in the alloy favored the formation of tin oxide, whereas lead favored the formation of a lead oxide film. Moreover, the analysis showed that the alloy had a higher reduction current than the use of single electrodes. The Faradaic efficiency was investigated at -2.0 V vs. the silver-silver chloride

electrode using an H type electrochemical cell. The highest FE obtained using the lead tin alloy was 79.8% for formate, which was 16% higher than the use of tin or lead electrodes.[57]

Platinum and palladium has been used as an alloy for electrochemical reduction of CO_2. Another study investigated the electrochemical reduction of carbon dioxide to formic acid at low overpotentials using a palladium/platinum catalyst on a carbon paper support, and compared the reduction reaction with the reverse oxidation reaction of formic acid to carbon dioxide.[58] The selection of the two metals was based on the high catalytic activity of the two metals individually.[58] Electrodeposited palladium layers on the platinum substrate exhibited a reduction in the formation rate for formic acid compared to the use of bulk palladium.[58] The palladium-platinum nanoparticles have a low reduction potential of carbon dioxide to formate at 0 V which approaches the theoretical equilibrium potential of +0.02 V vs. the NHE. Moreover, the use of Pd(70%):Pt(30%) alloy exhibited a formic acid FE of 88% after electrolysis for 1 hour at -0.4 V. The combination of the two metals also allowed for the reverse oxidation of formic acid to carbon dioxide at the electrode. However, the formation of formic acid was limited by the formation of a carbon monoxide film at the catalyst surface.[58]

This recent example of carbon supported catalyst points to the need for reducing the over potential needed for electrochemical reduction of CO_2 and address CO poisoning of catalysts supported on carbon. This research work pursued using hydrogen molybdenum films to lower the required overpotential and potential for reducing the effect of CO poisoning. Additionally, the films may be more selective for formate. Hydrogen molybdenum bronze films were prepared by electrodeposition of peroxymolybdic acid. Carbon dioxide was electrochemically reduced to formate and quantified by ion chromatography. The amount of formate and charge was used to calculate FE. Interestingly, this research shows that using a hydrogen molybdenum

bronze film resulted in reduction of CO_2 to formate with 8% FE at an applied potential of -0.4 V vs the silver/silver chloride (Ag/AgCl) reference electrode. While the FE for formate is low, this applied potential was found to be similar to using formate dehydrogenase as an electrocatalyst for reduction of CO_2 to formate.

CHAPTER 2

METHODOLOGY

Chemicals and Materials

Chemicals used were 3% hydrogen peroxide purchased locally, ITO glass substrates (14 Ω/square) purchased from Deposition Research Inc, carbon dioxide and nitrogen gas from Airgas. A 3.6 mM sodium carbonate solution was used as the eluent for ion chromatography. Sodium bicarbonate, sodium hydroxide, carbon paper with a resistivity of 80 mΩ·cm, fritted salt bridges, and sodium molybdate dihydrate were purchased from VWR and used as received. Formate standard, (1,000 ppm) was provided by Metrohm.

Equipment

A CHI 604E electrochemical work station with CHI software version 15.08 was used for all electrochemical deposition and reduction experiments. All potentials are reported using the silver/silver chloride reference electrode. Electrochemical reduction was carried out using two beakers containing the electrolyte connected by a salt bridge containing 1.0 M $NaSO_4$. An H-type electrochemical cell (VWR) was also utilized for electrochemical reduction of CO_2 to determine CO in the headspace. In all experiments the hydrogen molybdenum bronze film electrodeposited on carbon paper was the working electrode, the silver/silver chloride electrode was the reference and a platinum disc (2 mm) served as the counter electrode.

Electrodeposition of Hydrogen Molybdenum Bronze Films

Hydrogen molybdenum bronze films were prepared by electrodeposition on ITO and carbon paper. Sodium molybdate dihydrate, 2.5 g, was dissolved in 50 mL of deionized water and 11 mL of 3% hydrogen peroxide was added. This results in a yellow solution that was stirred for 24 hours. After turning clear, an additional 11 mL of 3% hydrogen peroxide was added. The

solution was adjusted to a pH of 2 using a calibrated Vernier® pH electrode by adding concentrated sulfuric acid dropwise. until a pH of 2 measured. The yellow peroxymolybdic acid solution was used for deposition of hydrogen molybdenum bronze films. A three electrode system was used in this experiment. The silver/silver chloride referene electrode was used as a reference, a 2 mm platinum disk was the counter electrode and the carbon paper or ITO was the working electrode. Bulk electrolysis reduced peroxymolybdic acid to a blue hydrogen bronze film on ITO or carbon paper using an applied potential of -2.0V. Separate films were deposited for 150, 300, 700 and 1,400 seconds. Films were prepared on ITO and sent for film thickness measurements as well as X-ray Photoelectron Spectroscopy (XPS). Characterization of films deposited on carbon paper is ongoing.

<div align="center">Characterization of Films</div>

Film thickness measurements and conductivity were performed by Dr. Toby Nelson at Oklahoma State University. The four-point probe method was used to measure electrical conductivity of the thin films. Resistance was measured using a Lucas Labs Pro 4-point probe connected to a Keithley 2400 source meter. Film thickness was measured using a Bruker DektakXT® Stylus Profiler. This instrument uses deflection of a cantilever to determine thickness. X-Ray Photoelectron Spectroscopy was performed by Dr. Nicholas Materer also at Oklahoma State University. The XPS measurements were carried out using the Mg anode of a PHI 300W twin anode X-ray source and a PHI double pass cylindrical mirror analyzer having a pass energy of 50 eV. X-Ray Diffraction of films was performed by Dr. Dwight Myers at East Central University using a Bruker D2 Phaser X-Ray Diffractometer.

Electrochemical Reduction of CO_2

The electrolyte, 0.1 M $NaHCO_3$, was used with the hydrogen bronze films on carbon paper for electrochemical reduction of CO_2. Figure 2 shows two beakers and a fritted salt bridge which was filled with 0.1 M Na_2SO_4 to connect the anode and cathode.
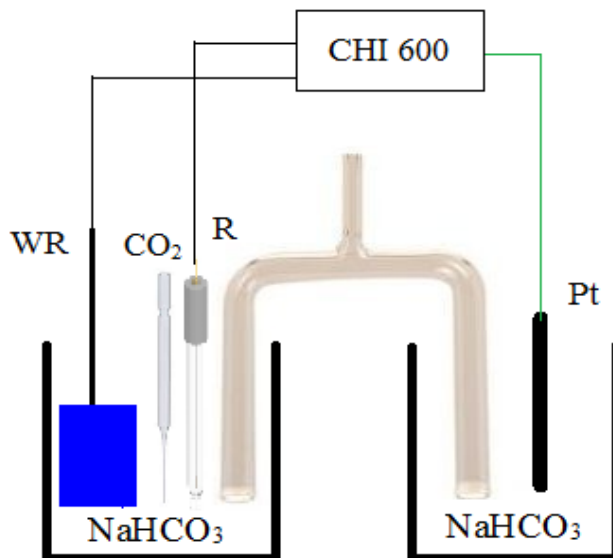
Figure 2. The electrochemical cell used for CO_2 reduction experiments

The cathode beaker includes the reference electrode, hydrogen bronze film (working electrode) and 0.1 M $NaHCO_3$ or blue peroxymolybdic acid solution as supporting electrolyte mixed by bubbling CO_2. The anode was a 2 mm platinum disc electrode in 20 mL of 0.1 M of $NaHCO_3$ magnetically stirred. During that time, applied potentials used were -0.2, -0.4, -0.6, -0.8, -1, -1.2, and -1.4 V. The CHI software plotted current, time and integrated the data providing total charge in Coulombs.

Ion Chromatography Quantifying Formate

A 930 Metrohm ion chromatogram was used to analyze for formate. Metrohm Application Note S-260 used a Metro Sep a Supp 16-250/4.0 column at 45°C and at a flow rate of 0.7 mL/minute Sodium carbonate, 3.6 mmol is the eluent and 5 mM H_2SO_4 chemically suppresses the conductivity.[15] Standards of formate were prepared by diluting with 0.1 M $NaHCO_3$. Formate is identified at 4.6 minutes and peak area was used to quantify formate. The background was determined by bubbling both nitrogen and carbon dioxide into the electrolyte for one hour without an applied potential.

GC Analysis for Carbon Monoxide

An H-type electrochemical cell was sealed with three-hole stoppers containing the reference and hydrogen bronze film on the left and platinum counter electrode on the right. Figure 3 shows the electrochemical cell setup used for sampling the headspace for GC analysis to determine CO. An applied potential of –0.4V was used due to finding the most amount of formate at this applied potential. The amount of CO at other potentials are ongoing experiments. The headspace was analyzed by GC for carbon monoxide.

Figure 3: Sealed electrochemical H cell for CO determination

CHAPTER 3

RESULTS AND DISCUSSION

Film Characterization: Film Thickness

Electrodeposition of the films was carried out at -2.0 V in the yellow peroxymolybdic acid solution using bulk electrolysis. Films were prepared on ITO for XPS and film thickness measurements while films prepared on carbon paper were used for electrochemical reduction experiments. Figure 4 shows the carbon paper film before electrodeposition and Figure 5 shows the film after 100 seconds of electrodeposition. While the blue color is difficult to see in Figure 6, electrodeposition on ITO results in a blue film that is easier to see as shown in Figure 6.
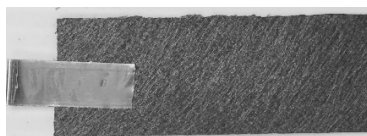
Figure 4: Carbon paper before the electrodeposition
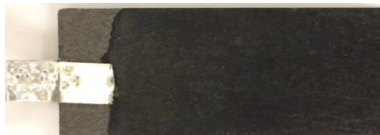
Figure 5: Hydrogen molybdenum bronze film after 100 seconds of electrodeposition on carbon paper

Figure 6: Hydrogen molybdenum bronze film on ITO after 100 seconds of electrodeposition showing the blue color of the film

Table 2 lists the time of electrodeposition and measured hydrogen molybdenum bronze film thickness measurements provided by Dr. Toby Nelson using a Bruker DektakXT® Stylus Profiler.

Table 2. Film thickness measurements (µm) of the electrodeposited films on ITO versus time

Time(s)	Thickness (µm)	Error (± µm)
100	129	16
300	142	4
700	194	6
1400	462	17

As time of deposition increases so does film thickness. One goal was to be able determine how long to deposit films for to obtain a desired thickness as this relationship is not known. This led to a linear plot fitting thickness and time as shown in Figure 7.
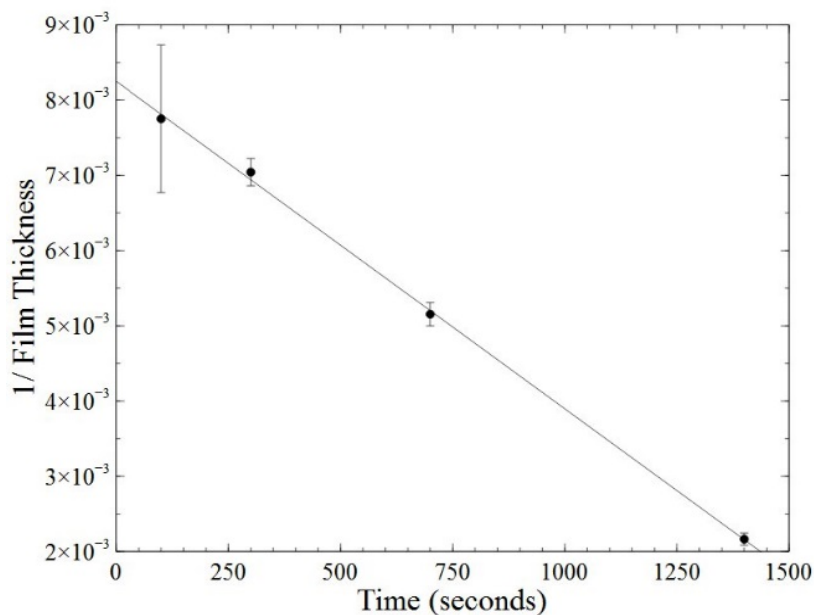
Figure 7: Plot of inverse film thickness (µm) versus time (s)

Equation (11) below is the linear fit with an R^2 value of 0.9995.

29

$$\mu m^{-1} = -4.4 \times 10^{-6} (\frac{\mu m^{-1}}{s})t + 825.2 \mu m^{-1} \qquad (11)$$

The error bar at 100 seconds is large in this plot due to a small thickness and a typical error of 6-17 μm. This results in a much larger error at lower films thicknesses compared to the error of thicknesses measured after 1,400 seconds of electrodeposition. Within error, the plot of inverse film thickness with time is linear indicating that electrodeposition is a second order process.

<u>Film Characterization: Film Conductivity</u>

One significant parameter of an electrocatalytic film is that the film be conductive. If the film acts as an insulator, this will cause an undesirable impedance or inhibit the exchange of electrons. Sheet resistance measurements were obtained by using a 4-point probe and reported in units of Ω/square. Table 3 below shows the sheet resistance of the films as the function of deposition time.

Table 3. Conductivity of the hydrogen bronze film as a function of deposition time

Time(s)	Sheet Resistance (Ω/square)	Error (± Ω/square)
100	3.63	0.03
300	3.81	0.02
700	3.31	0.03
1400	3.58	0.04

While film thickness ranges from 129-462 μm, the sheet resistance is the same in this range. There are two reasons that account for this result. In one situation the four points of the probe reached the ITO substrate. In this case the sheet resistance should match the value of the ITO layered substrate given by the manufacturer, 14 Ω/square. The second possibility is that the electrodeposited sheet film resistance is independent of film thickness. The four point probe

measurements result in a sheet resistance less than the ITO layer. This supports the fact that the

hydrogen molybdenum bronze films resistance was measured and not the ITO layer.

<div align="center">Film Characterization: XPS and XRD</div>

X-Ray Photoelectron Spectroscopy was used to characterize the electrodeposited films.

Figure 8 shows the XPS and assigned peaks confirming that molybdenum and oxygen are

present. When hydrogen is present in the molybdenum oxide lattice, the film is known to be a

blue color.[15, 17] Hydrogen can not be determined by XPS. Experiments are ongoing to determine

the hydrogen content in the films using Rutherford Backscattering.   Carbon paper with and

without electrodeposited films was also analyzed by X-Ray Diffraction shown in Figure 9.
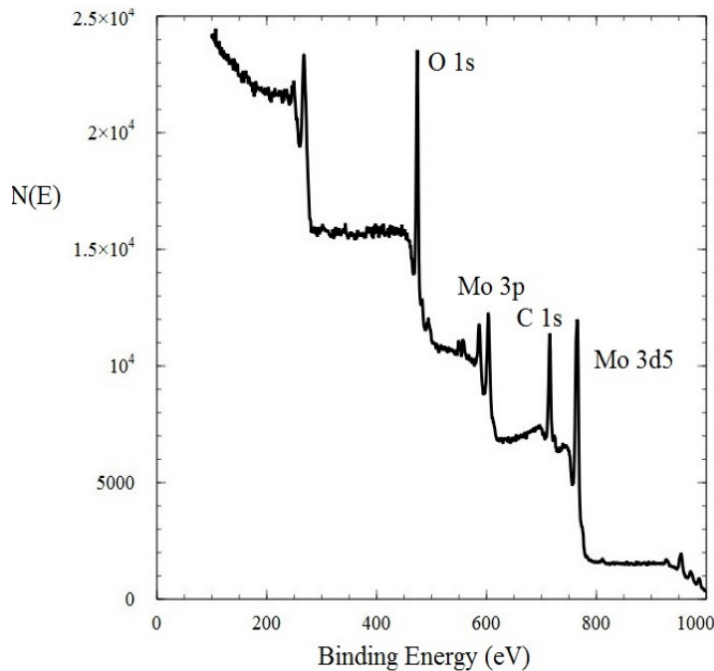
Figure 8: The XPS spectrum of the electrodeposited hydrogen molybdenum bronze film
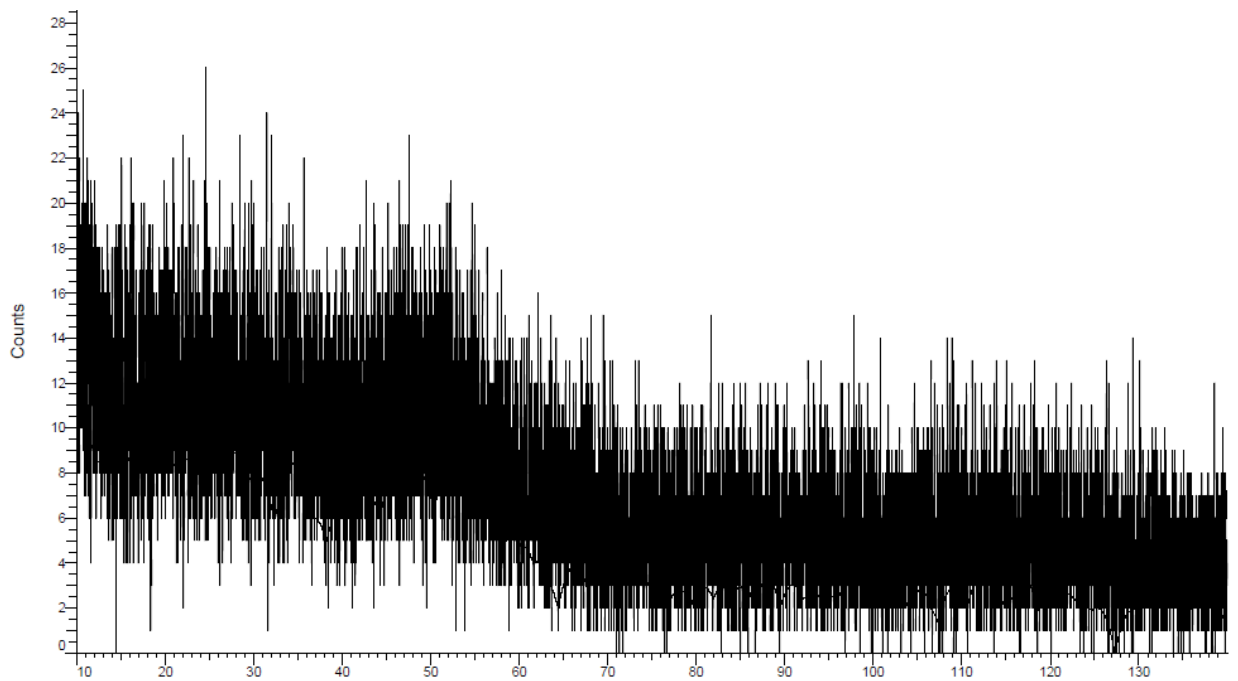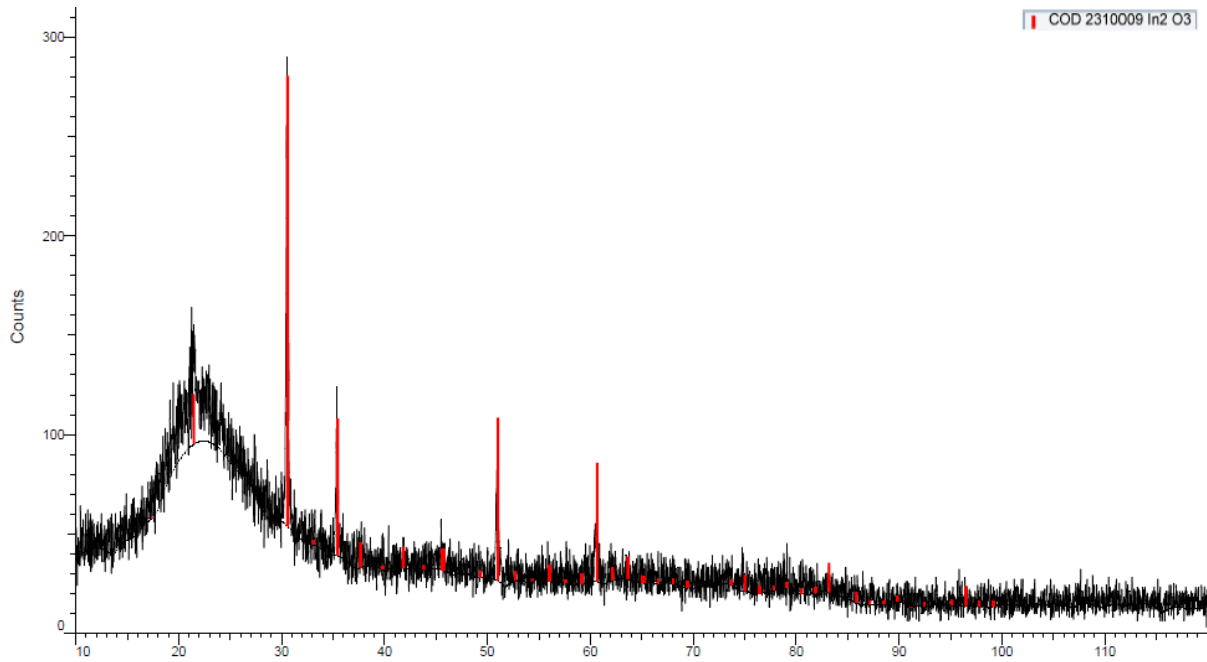
Figure 9: X-Ray Diffraction of conductive carbon paper only (top) and the deposited hydrogen bronze film (bottom)

The carbon paper only shows a broad peak at approximately 20°. The carbon paper with electrodeposited film however shows no clear peak meaning that the film amorphous.

<u>Film Characterization: Cyclic Voltammetry</u>

Cyclic voltammetry of the hydrogen bronze film on carbon paper was attempted in 0.5 M
H_2SO_4 to study hydrogen intercalation. After a few cycles, the film completely dissolved into
the bulk solution. There were no clear oxidation or reduction peaks. This result is consistent
with experiments that confirm oxidation of electrodeposited films results in mass loss of the
film.[59]

<u>Cyclic Voltammetry of CO_2 Reduction</u>

Figure 10 shows the CV of carbon paper in nitrogen and CO_2 saturated 0.1 M $NaHCO_3$,
while Figure 11 is the same experiment using electrodeposited films on carbon paper.
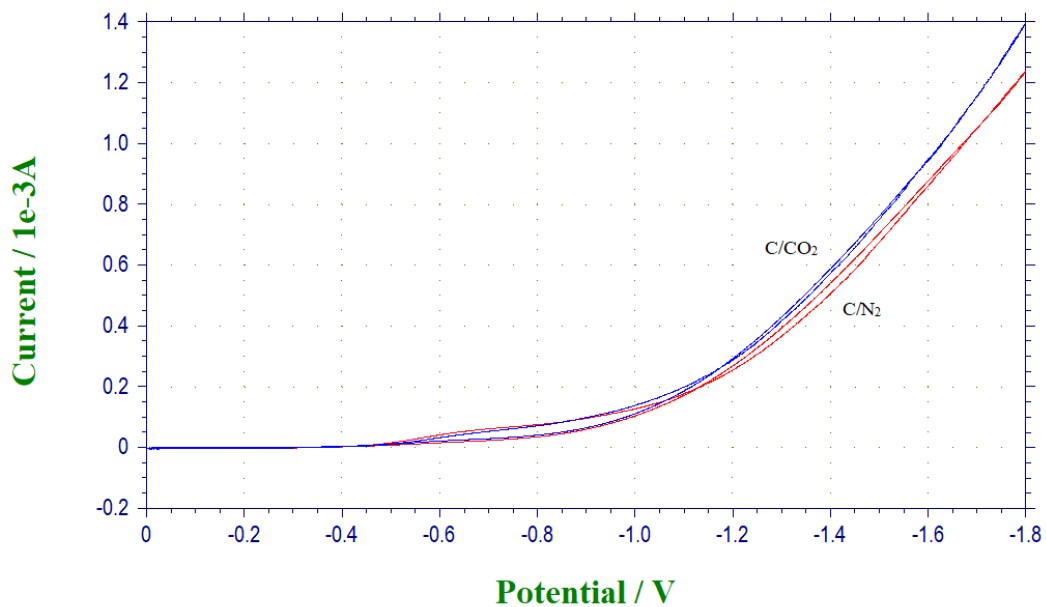
Figure 10. The CV of carbon paper in nitrogen and CO_2 saturated 0.1 M $NaHCO_3$ using the
silver chloride as a reference electrode
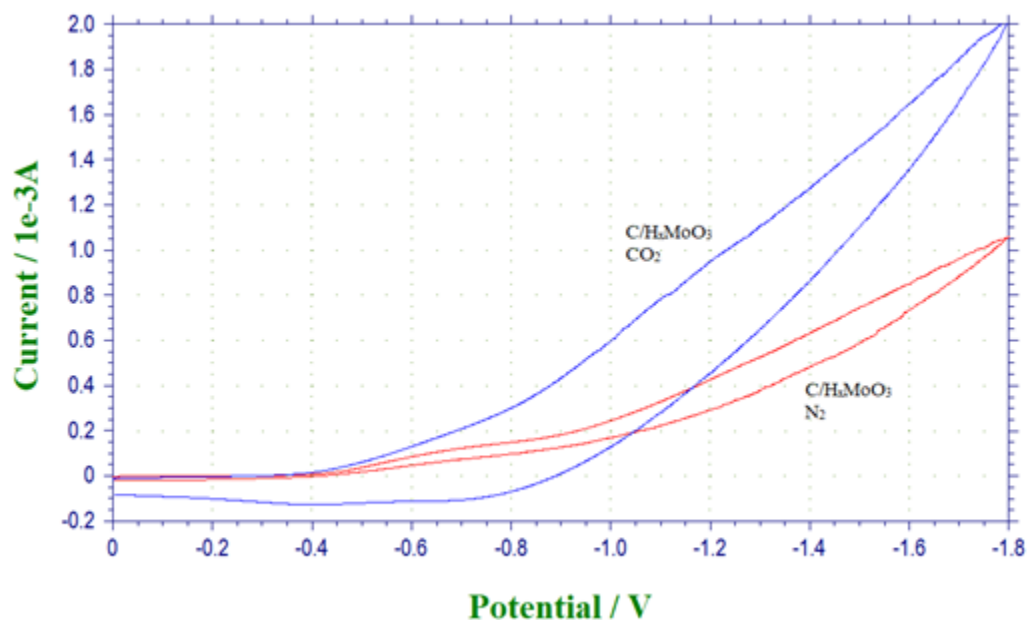
Figure 11. The CV of carbon paper with the hydrogen molybdenum bronze film in nitrogen and CO_2 saturated 0.1 M $NaHCO_3$ using the silver chloride as a reference electrode

Figure 10 shows that there is no increase in current using carbon paper when the electrolyte is saturated with CO_2 compared to that of nitrogen. However, Figure 11 shows that the onset of reduction of CO_2 starts at an applied potential of -0.4 V. This is evident by an increase in current compared to the CV of carbon paper and hydrogen molybdenum bronze film in nitrogen saturated electrolyte. As such, electrodeposited hydrogen molybdenum bronze films on conductive carbon carries out catalytic reduction. One possible product is formate which was quantified by ion chromatography using reduction potentials from -0.2 V to -1.4 V.

<u>Electrochemical Reduction of Carbon Dioxide and Quantifying Formate</u>

Figure 12 shows a typical ion chromatogram identifying formate in 0.5 M $NaHCO_3$.
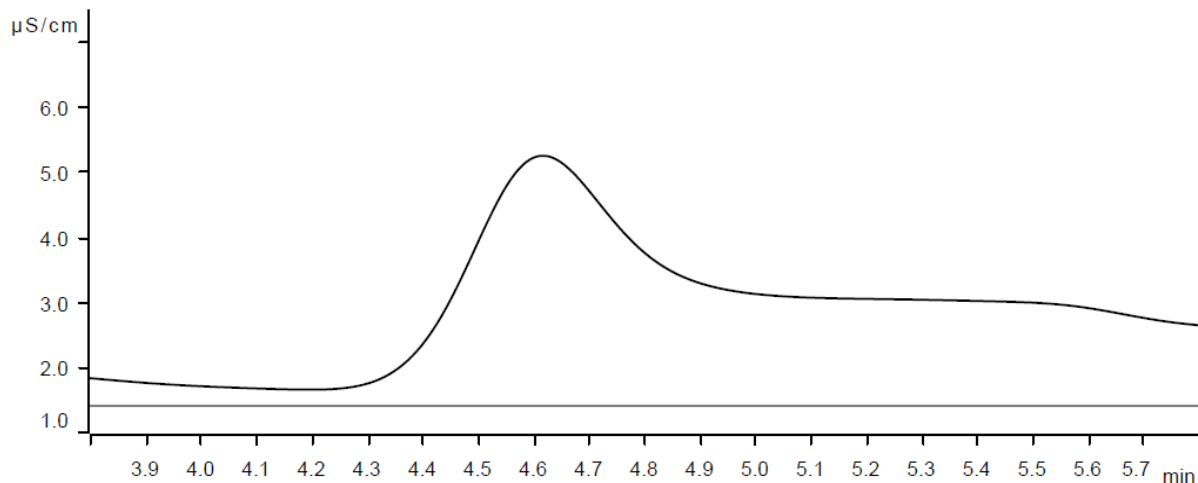
Figure 12: Typical ion chromatogram of conductivity (μS/cm) and time (minutes) identifying formate in 0.5 M NaHCO₃ with a retention time of 4.6 minutes

A 1,000 ppm solution of formate was diluted with 0.1 M NaHCO₃ to make standard solutions. The calibration of peak area and formate concentration is shown in Figure 13.

$$y = 3.1994\text{E-}02x - 1.6962\text{E-}03$$
$$R^2 = 9.9900\text{E-}01$$
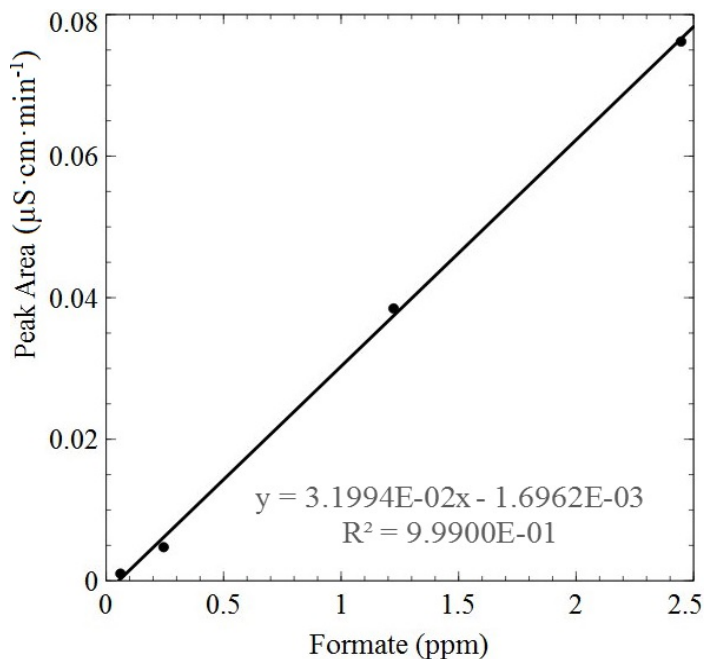
Figure 13: Calibration for determination of formate

Table 4 shows the applied potential, amount of formate (ppm), charge in Coulombs and

Faradaic efficiency. The equation for faradaic efficiency for reduction of CO_2 to formate is

shown below in Equation 12.[60]

$$\varepsilon = \frac{n_{formate}nF}{Q} \times 100\% \qquad (12)$$

where ε is Faradaic efficiency, F is Faraday's constant 96,485 Coulombs/mol, $n_{formate}$ is moles of

formate, n is two electrons for reduction of carbon dioxide to formate and Q is the charge in

coulombs for the duration of electrochemical reduction of CO_2.

Table 4. The applied potential using the silver chloride electrode as a reference, amount of formate (ppm), charge and FE for electrochemical reduction of CO_2

Potential (V)	Formate (ppm)	Charge (Coulombs)	Faradaic efficiency (%)
-1.4	0.23	26.44	0.07
-1.2	0.41	23.925	0.13
-1.0	0.96	9.66	0.93
-0.8	0.615	3.133	1.75
-0.6	0.286	0.55	4.67
-0.4	0.129	0.15	8.34
-0.2	0	0	0

Figure 14 is a plot of Faradaic efficiency and applied potential to the working electrode.
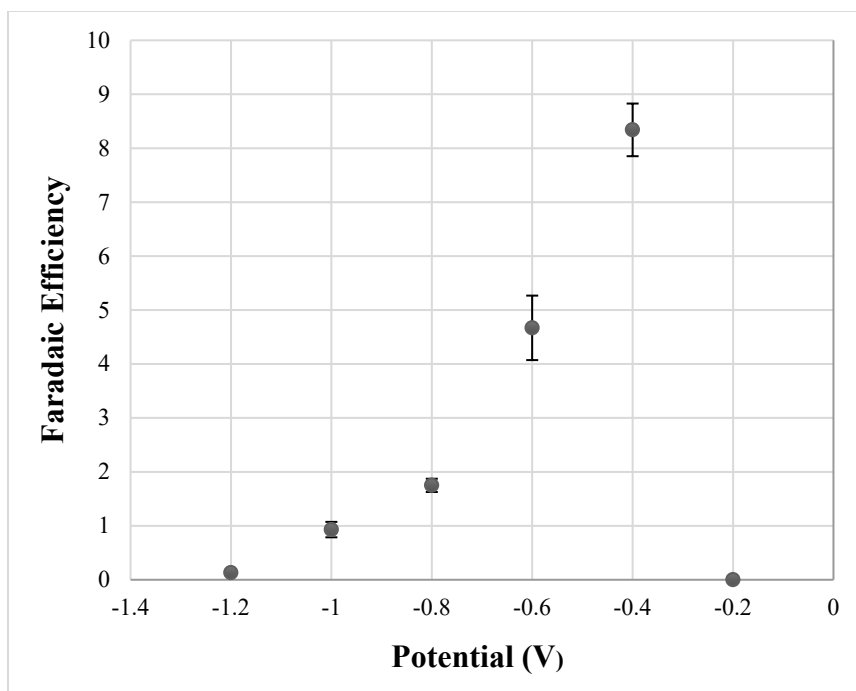
Figure 14. Faradaic efficiency (%) plotted against applied potential

These results show that the hydrogen molybdenum bronze film is catalytic for reduction of carbon dioxide. A maximum amount of formate was obtained at -1.0 V (0.96 ppm). The reduction potential for CO_2 to formate vs the RHE at a pH of 8.3 is calculated to be +0.054 V.[46] An applied potential of -0.4 V vs the silver/silver chloride reference corresponds to +0.3 V vs the RHE. This potential is much more positive compared to use of palladium and platinum alloys deposited on carbon, -0.5 V vs the RHE.[58] Interestingly, formate dehydrogenase is known to contain molybdenum and tungsten active sites for reduction of CO_2 to formate.[61] Formate dehydrogenase was used as an electrocatalyst for reduction of CO_2 to formate. In a solution of 10 mM CO_2 and formate buffered to a pH of 8.0 the reduction potential was found to be approximately -0.45 V vs the SHE.[62] The reduction potential becomes more positive as the pH decreases from 8.0 to 6.0. A similar study using formate dehydrogenase at a pH of 6.5 resulted in a maximum FE for reduction of CO_2 to formate using an applied potential of -0.41 V vs. the

SHE.[61] In this work a maximum FE for formate was obtained at -0.4 V (-0.165 V vs SHE). This is more positive compared to use of formate dehydrogenase likely due to carrying out reduction of CO_2 at a pH of 8.3. This result indicates that the electrodeposited hydrogen molybdenum bronze films are likely capable of biomimicking formate dehydrogenase due to containing molybdenum as an active metal site for electrochemical reduction. In this work a maximum FE was obtained at -0.4 V (8.34 %). Compared to Table 1, this result matches the lowest FE obtained using ruthenium electrocatalysts. Future strategies are aimed at improving the faradaic efficiency of electrodeposited hydrogen bronze films toward CO_2 reduction to formate. Headspace analysis of the electrochemical cell is critical to show that hydrogen bronze films electrodeposited on carbon paper may prevent CO poisoning.

Determining Headspace CO

The H type cell was used to attempt investigating the amount of CO generated in the electrochemical reduction of CO_2. The 0.1 M $NaHCO_3$ solution was saturated with CO_2, sealed with a stopper and magnetically stirred with an applied potential of -0.4 V for reduction due to finding the highest amount of formate. The headspace was analyzed for CO. Due to CO being detected in air, three measurements were performed to determine if electrochemical reduction resulted in CO. The first measurement purged the electrochemical cell with CO_2, sealed with a stopper and the headspace sampled to determine background CO. The second measurement followed the same steps adding carbon paper with no hydrogen bronze film as the working electrode and reducing CO_2. The third measurement repeated reduction of CO_2 using the hydrogen molybdenum bronze film on carbon paper. During these experiments, the discovery was made that the sensitivity for CO in the presence of CO_2 is significantly reduced complicating the quantification of CO in the headspace. Towards this goal, methods for detection of CO and

38

other products are ongoing. This effort includes experiments carrying out reduction of CO_2 for longer periods of time and other detection methods for CO_2. One such example is the MQ-7 CO sensor.

CHAPTER 4

CONCLUSIONS

The purpose of this research work was to prepare hydrogen molybdenum bronze films using electrodeposition and carry out electrochemical reduction of CO_2. A yellow peroxymolybdic acid solution was prepared by dissolving sodium molybdate dihydrate in water and adding hydrogen peroxide. After adjusting to an acidic pH and adding more hydrogen peroxide, this resulted in a stable yellow peroxymoybdic acid solution for electrodeposition of hydrogen bronze films. The carbon paper and/or glass/ITO substrates were used to carry out bulk electrolysis at -0.7 V vs. the silver chloride reference electrode to deposit the hydrogen molybdenum bronze films. Deposition was carried out at different times ranging from 100 to 1,400 seconds. The thickness of the films was approximately 200-500 μm. The inverse of film thickness vs. time was found to be a linear. This fit allowed determining film thickness simply based on time of electrodeposition.

The resistance of the electrodeposited hydrogen molybdenum bronze films was found to be approximately 4 Ω/square, which is less than ITO coated glass, 14 Ω/square. This confirmed that the resistance measurement was directly of the electrodeposited film and not the resistance of the conductive substrate. The presence of molybdenum and oxygen was confirmed by using XPS. Hydrogen is also present in these films. Experiments are ongoing using Rutherford Backscattering to quantify hydrogen content in the electrodeposited hydrogen molybdenum bronze films. There were no clear peaks present in XRD of the films on carbon paper. This indicated that the prepared hydrogen molybdenum bronze films were amorphous in nature meaning not crystalline. Future work includes electrodeposition for longer times to determine the effect on crystalline structure.

The films were found to be catalytic toward the electrochemical reduction of carbon dioxide. Cyclic voltammetry was carried out using both carbon paper only and carbon paper with hydrogen bronze films in nitrogen saturated and carbon saturated 0.1 M $NaHCO_3$ electrolyte. Compared to carbon paper only, when using the hydrogen molybdenum bronze film as the working electrode, an increase in measured current occurs at an applied potential of -0.4 V vs. the silver chloride reference electrode indicating catalytic reduction of CO_2 is occurring. In using hydrogen bronze films on carbon paper, the highest FE was 8% at an applied potential of -0.4 V using the silver chloride reference. At more negative potentials the Faradaic efficiency decreases but the measured current compared to using carbon paper with a hydrogen molybdenum bronze film in nitrogen electrolyte increases. Interestingly, an applied potential of -0.4 V matches electrocatalytic work using formate dehydrogenase as an electrocatalyst. This is due to the molybdenum active site of the enzyme. This result indicates that the electrodeposited hydrogen molybdenum bronze film is capable of biomimicking formate dehydrogenase.

Measuring headspace for CO was attempted at an applied potential of -0.4 V vs. the silver chloride reference electrode using a sealed H type electrochemical cell. Analysis of the headspace initially revealed that there was no CO. However, the method suffers from significantly reduced sensitivity to CO in the presence of CO_2 and experiments are ongoing.

While the FE for formate is low compared to other literature results, these films are cheap and easy to prepare. Ongoing experiments include measuring CO at applied potentials, carrying out reduction under neutral and acidic conditions as well as using tungsten to carry out ion exchange with hydrogen which should improve the biomimicking capabilities of the electrodeposited bronze film. The expectation is an improved Faradaic efficiency reducing CO_2 to formate.

REFERENCES

1. Xiaoquan, M.; Kanan. M. W. Pd-Catalyzed Electrohydrogenation of Carbon Dioxide to Formate: High Mass Activity at Low Overpotential and Identification of the Deactivation Pathway. J. Am. Chem. Soc. 2015, 14, 4701-4708. doi:10.1021/ja511890h (accessed May 5, 2019).

2. Li, X. P.; Xiang, X. D.; Yang, H. Y.; Weishan, Ll. Hydrogen Tungsten Bronze-Supported Platinum as Electrocatalyst for Methanol Oxidation. Fuel Cells. 2013, 13, 314–318., doi:10.1002/fuce.201000131 (accessed May 5, 2019).

3. Pathan, H. M.; Min, S. K.; Jung, D. K.; Joo, O. S. Electrosynthesis of molybdenum oxide thin films onto stainless substrates. E-chem. Comms. 2006, 8, 273-278. http://www.sciencedirect.com/science/article/pii/S1388248105003711 (accessed May 5, 2019).

4. Kwong, W. L.; Qiu, H.; Nakaruk, A.; Koshy, P.; Sorrell, C. C., Photoelectrochemical Properties of WO_3 Thin Films Prepared by Electrodeposition. Energy Procedia. 2013, 34, 617-626.

5. Koçak, S.; Ertaş, F. N.; Dursun, Z., Electrochemical deposition and behavior of mixed-valent molybdenum oxide film at glassy carbon and ITO electrodes. Applied Surface Science 2013, 265, 205-213.

6. Baoxing, W.; Shaojun, D., Electrocatalytic properties of mixed-valence molybdenum oxide thin film modified microelectrodes. J. Electroanal. Chem. 1994, 379, 207-214.

7. Kazusuke, Y. Electrodeposited Films from Aqueous Tungstic Acid-Hydrogen Peroxide Solutions for Electrochromic Display Devices, Jpn. J. Appl. Phys. 1987, 26, 1884. http://stacks.iop.org/1347-4065/26/i=11R/a=1884 (accessed May 5, 2019).

8. Kondrachova, L.; Benjamin, P. H.; Ganesh, V.; Williams, R. D.; Stevenson, K. J. Cathodic Electrodeposition of Mixed Molybdenum Tungsten Oxides from Peroxo-polymolybdotungstate Solutions. Langmuir. 2006, 22, 10490-10498. http://dx.doi.org/10.1021/la061299n (accessed May 5, 2019)

9. McEvoy, T. M.; Stevenson, K. J., Electrochemical quartz crystal microbalance study of the electrodeposition mechanism of molybdenum oxide thin films from peroxo-polymolybdate solution. Analytica Chimica Acta. 2003, 496, 39-51.

10. Materer, N. F.; Allen, A.; Evgueni, B. K.; Kashif, R. K.; Walter, C.; Kevin, H.; Eman, F. S. The preparation and chemical reaction kinetics of tungsten bronze thin films and nitrobenzene with and without a catalyst. Sur. Sci. 2016, 648, 345-351. http://www.sciencedirect.com/science/article/pii/S0039602815003702 (accessed May 5, 2019).

11. Chen, L.; Cooper, A. C.; Pez, G. P.; Cheng, H., On the Mechanisms of Hydrogen Spillover in MoO_3. J. Phys. Chem. C. 2008, 112, 1755-1758.

12. Hu, X. K.; Qian, Y. T.; Song, Z. T.; Huang, J. R.; Cao, R.; Xiao, J. Q., Comparative Study on MoO_3 and $HxMoO_3$ Nanobelts: Structure and Electric Transport. Chem. Mater. 2008, 20, 4, 1527-1533.

13. Sha, X.; Chen, L.; Cooper, A. C.; Pez, G. P.; Cheng, H., Hydrogen Absorption and Diffusion in Bulk α-MoO3. J. Phys. Chem. C. 2009, 113, 11399-11407.

14. Yin, H.; Kuwahara, Y.; Mori, K.; Che, M.; Yamashita, H. Plasmonic Ru/hydrogen molybdenum bronzes with tunable oxygen vacancies for light-driven reduction of p-nitrophenol. J. Mater. Chem. A. 2019, 7, 3783–3789.

15. Borgschulte, A. Sambalova, O. Delmelle, R. Jenastch, S. Hany, R. Nüesch, F. Hydrogen Reduction of Molybdenum Oxide at Room Temperature. Sci. Reports. 2017, 7, doi:10.1038/srep40761 (accessed May 5, 2019).

16. Wan, D. S.; Yusairie, M. Influence of pH Solution on the Electrodeposition of Tungsten Oxide (WO_3) Films onto Indium Tin Oxide (ITO)-glass Substrate. J. Sci. Tech. 2012, 4, 49-60.

17. Patel, K.j.; Panchal, C.; Kheraj, V.; Desai, M. S. Growth, Structural, Electrical and Optical Properties of the Thermally Evaporated Tungsten Trioxide (WO_3) Thin Films. Materials Chem. Phy. 2009, 114, 1, 2009, 475–478, doi:10.1016/j.matchemphys.2008.09.071 (accessed May 5, 2019).

18. Kadossov, E. B.; Apblett, W. A.; Materer, N. F.; Soutiani, A. R. Density-Functional Studies of Hydrogen Peroxide Adsorption and Dissociation on MoO_3(100) and $H_{0.33}MoO_3$(100) Surfaces. RSC Advances. 2015, 5, 118, 97755–97763, doi:10.1039/c5ra08006a (accessed May 5, 2019).

19. Macêdo, M. A.; Dall'Antonia, L. H.; Valla, B.; Aegeter, A. M. Electrochromic Smart Windows. J. Non-crystalline S. 1992, 147-148, 792–798., doi:10.1016/s0022-3093(05)80718-5 (accessed May 5, 2019).

20. Summers, D. P.; Steven, L.; Karl W. F. The electrochemical reduction of aqueous carbon dioxide to methanol at molybdenum electrodes with low overpotentials, J. Electroanalytical Chem. Interfacial Elec. 1986, 205, 219-232.

http://www.sciencedirect.com/science/article/pii/0022072886902330 (accessed May 5, 2019).

21. Ayyappan, S.; Rao, C. N. R. A Simple Method of Hydrogen Insertion In Transition Metal Oxides To Obtain Bronzes. Mater. Res. Bull. 1995, 30, 947-951.

22. Gui, Y.; Blackwood, D. J. Electrochromic Enhancement of WO_3-TiO_2 Composite Films Produced by Electrochemical Anodization, J. Electrochem. Soc. 2014, 161, E191-E201. http://jes.ecsdl.org/content/161/14/E191.abstract (accessed May 5, 2019).

23. Ressler, T.; Wienold, J.; Jentoft, R. E. Formation of Bronzes during Temperature programmed Reduction of MoO_3 with Hydrogen-An In situ XRD and XAFS Study. Solid State Ionics. 2001, 141-142, 243-252.

24. Shen P. K.; Syed, J. B.; Tseung, A. C. C. The Performance of Electrochromic Tungsten Trioxide Films Doped with Cobalt or Nickel. J. Electrochem. Soc.1990, 138, 2778-2783.

25. Pauporté, T. A Simplified Method for WO_3 Electrodeposition, J. Electrochem. Soc. 2002, 149, C539-C545. http://jes.ecsdl.org/content/149/11/C539.abstract (accessed May 5, 2019).

26. Baeck, S. H.; Jaramillo, T.; Stucky, G. D.; Mcfarland, E. W. Controlled Electrodeposition of Nanoparticulate Tungsten Oxide. Nano Letters. 2002, 2, 831-834. http://dx.doi.org/10.1021/nl025587p (accessed May 5, 2019).

27. Kublanovsky, V.; Bersirova, O.; Yapontseva, Y.; Cesiulis, H.; Murphy, P. E. Cobalt-molybdenum-phosphorus alloys: Electroplating and corrosion properties, Protection Met. Phys. Chem. Surfaces. 2009, 45, 588-594. http://dx.doi.org/10.1134/S2070205109050165 (accessed May 5, 2019).

28.   Huang, Y. J.; Dai, H. H.; Li, W. S.; Li, G. L.; Shu, D.; Chen, H. Y. Electrodeposition
        preparation of Pt–H_xWO_3 composite and its catalytic activity toward oxygen reduction
        reaction, J. Power Sources. 2008, 184, 348-352.
        http://www.sciencedirect.com/science/article/pii/S0378775308006411 (accessed May 5,
        2019).

29.   Taube, F.; Masato, H.; Ingegärd, A.; Lage, P. Characterisation of aqueous
        peroxomolybdate catalysts applicable to pulp bleaching. J. Am. Chem. Soc. 2002, 1002–
        1008.

30.   Abraham, J. Scientists Study Ocean Absorption of Human Carbon Pollution. The
        Guardian, https://www.theguardian.com/environment/climate-consensus-97-per-
        cent/2017/feb/16/scientists-study-ocean-absorption-of-human-carbon-pollution. (accessed
        May 5, 2019)

31.   Zhenzhu, X.; Yanling, J.; Guangsheng, Z. Response and Adaptation of Photosynthesis,
        Respiration, and Antioxidant Systems to Elevated CO_2 with Environmental Stress in
        Plants. Front. Plant Sci. 2015, 6, 701, https://www.ncbi.nlm.nih.gov/pubmed/26442017
        (accessed May 5, 2019).

32.   National Oceanic and Atmospheric Administration. "How Does Sea Ice Affect Global
        Climate?". Oceanservice https://oceanservice.noaa.gov/facts/sea-ice-climate.html.

33.   Izumi, Y. Recent Advances in the Photocatalytic Conversion of Carbon Dioxide to Fuels
        with Water and/or Hydrogen Using Solar Energy and Beyond. Coordination Chem. Rev.
        2013, 257, 1, 171–186.
        https://www.sciencedirect.com/science/article/abs/pii/S0010854512001002 (accessed
        May 5, 2019).

34. Fogarty, D. Study: Global CO_2 Emissions to Hit Record in 2018. The Straits Times, https://www.straitstimes.com/world/study-global-co2-emissions-to-hit-record-in-2018 (accessed May 5 ,2019)

35. Carrington, D. Brutal News: Global Carbon Emissions Jump to All-Time High in 2018 The Guardian, https://www.theguardian.com/environment/2018/dec/05/brutal-news-global-carbon-emissions-jump-to-all-time-high-in- 2018(accessed May 5 ,2019)

36. Projected CO_2 Emissions Worldwide 2050. Statista, https://www.statista.com/statistics/263980/forecast-of-global-carbon-dioxide-emissions/ (accessed May 5, 2019).

37. Stein, T. Another Climate Milestone on Mauna Loa. Research.noaa.gov/article/ArtMID/587/ArticleID/2362/Another-climate-milestone-falls-at-NOAA's-Mauna-Loa-observatory (accessed May 5, 2019)

38. Joglekar, M.; Nguyen, V.; Pylypenko, S.; Ngo, C.; Li, Q.; O'Reilly, M. E.; Gray, T. S.; Hubbard, W. A.; Gunnoe, T. B.; Herring, A. M.; Brian, G. Trewyn. Organometallic Complexes Anchored to Conductive Carbon for Electrocatalytic Oxidation of Methane at Low Temperature. J. Am. Chem. Soc. 2015, 138 , 116–125

39. Brown, Theodore E., LeMay, Eugene H., Bursten, Bruce E.,Burdge, Julia R. Chemistry: The Central Science; Prentice Hall: Upper Saddle River, New Jersey. 2012, 1045-1046.

40. Yang, N.; Siegfried R. W.; Xin, J. Electrochemistry of Carbon Dioxide on Carbon Electrodes. ACS Applied Mat. Interfaces. 2016, 8, 42, 28357–28371.

41. Miller, H.; Passaglia, E.; Vizza, F.; Pucci, A.; Bartoli, C.; Pagliaro, V.; Bellini, M.; Marchionni, A.; Jacopo, R. Improving the Energy Efficiency of Direct Formate Fuel Cells with a Pd/C-CeO_2 Anode Catalyst and Anion Exchange Ionomer in the Catalyst

Layer. Energies. 2018, 11, 2, 369. https://www.mdpi.com/1996-1073/11/2/369 (accessed May 5, 2019).

42. An, L.; Chen, R. Direct Formate Fuel Cells: A Review. J. Power Sources. 2016, 320, 127–139. https://www.sciencedirect.com/science/article/abs/pii/S0378775316304438 (accessed May 5, 2019).

43. Song, Y.; Rui, P.; Dale, K. H.; Bonnesen, P. V.; Liangbo, L. Zili, W.; Meyer, H. M.; Miaofang, C.; Cheng, M.; Sumpter, B. G.; Rondinone, A. J. High-Selectivity Electrochemical Conversion of CO_2 to Ethanol Using a Copper Nanoparticle/N-Doped Graphene Electrode. Chem. 2016, 1, 19, 6054.

44. Kaneco, S.; Katsumata, H.; Suzuki, T.; Ohta, K.. Electrochemical reduction of CO_2 to methane at the Cu electrode in methanol with sodium supporting salts and its comparison with other alkaline salts. Energy Fuels. 2006, 20, 1, 409-414.

45. Feaster, J. T.; Chuan, S.; Etosha, C. R.; Toru, H., David N. A., Kuhl, P. H.; Hahn, C.; Korskov, J.; Jaramillo, F. T. Understanding Selectivity for the Electrochemical Reduction of Carbon Dioxide to Formic Acid and Carbon Monoxide on Metal Electrodes. ACS Catal. 2017, 7, 7, 4822-4827.

46. Kortlever, R.; Shen, J.; Schouten, P. J. K.; Vallejo, C. F.; Koper. M. T. M. Catalysts and Reaction Pathways for the Electrochemical Reduction of Carbon Dioxide. J. Phys. Chem. Letters 2015, 6, 20, 4073-4082.

47. Hossain, M. N.; Zhonggang, L.; Jiali, W.; Aicheng, C. Enhanced Catalytic Activity of Nanoporous Au for the Efficient Electrochemical Reduction of Carbon Dioxide. Appl. Catal., B: Environ. 2018, 236, 483-489.

48. Fang, Y. Flake, C. J. Electrochemical Reduction of CO_2 at Functionalized Au Electrodes. J. Am. Chem. Soc. 2017, 139, 9, 3399-3405.

49. Sreekanth, N.; Kanala, L. P. Selective Reduction of CO_2 to Formate through Bicarbonate Reduction on Metal Electrodes: New Insights Gained from SG/TC Mode of SECM. Chem. Commun. 2014, 50, 11143-11146.

50. Li, C. W.; Kanan. M. W. CO_2 Reduction at Low Overpotential on Cu Electrodes Resulting from the Reduction of Thick Cu2O Films. J. Am. Chem. Soc. 2012, 134, 17, 7231-7234.

51. Jiang, B.; Zhang, X. G.; Jiang, K.; Wu, D. Y.; Cai, W. B. Boosting Formate Production in Electrocatalytic CO_2 Reduction over Wide Potential Window on Pd Surfaces. J. Am. Chem. Soc. 2018, 140, 8, 2880-2889.

52. Elgrishi, N.; Chambers, B. M. Xia, W.; Marc, F. Molecular Polypyridine-based Metal Complexes as Catalysts for the Reduction of CO_2. Chem. Soc. Rev. 2017, 46, 3, 761-796.

53. Min, X.; Kanan, M. W., Pd-Catalyzed Electrohydrogenation of Carbon Dioxide to Formate: High Mass Activity at Low Overpotential and Identification of the Deactivation Pathway. J. Am. Chem. Soc. 2015, 137, 14, 4701-4708.

54. Klinkova, A.; De Luna, P.; Dinh, C.-T.; Voznyy, O.; Larin, E. M.; Kumacheva, E.; Sargent, E. H., Rational Design of Efficient Palladium Catalysts for Electroreduction of Carbon Dioxide to Formate. ACS Catal. 2016, 6, 8115-8120.

55. Shinagawa, T.; Larrazábal, G. O.; Martín, A. J.; Krumeich, F.; Pérez-Ramírez, J., Sulfur-Modified Copper Catalysts for the Electrochemical Reduction of Carbon Dioxide to Formate. ACS Catal. 2018, 8, 837-844.

56.   Hu, X.-M.; Hval, H. H.; Bjerglund, E. T.; Dalgaard, K. J.; Madsen, M. R.; Pohl, M.-M.; Welter, E.; Lamagni, P.; Buhl, K. B.; Bremholm, M.; Beller, M.; Pedersen, S. U.; Skrydstrup, T.; Daasbjerg, K., Selective CO_2 Reduction to CO in Water using Earth-Abundant Metal and Nitrogen-Doped Carbon Electrocatalysts. ACS Catal. 2018, 6255-6264.

57.   Choi, S. Y.; Soon, K. J.; Kim, H. J.; Baek, I. L.; Park, K. T. Electrochemical Reduction of Carbon Dioxide to Formate on Tin–Lead Alloys. ACS sustainable. Chem. Eng. 2016, 4, 1311-318.

58.   Kortlever, R.; Ines, P.; Sander, K.; Koper, M. T. M. Electrochemical CO_2 Reduction to Formic Acid at Low Overpotential and with High Faradaic Efficiency on Carbon-Supported Bimetallic Pd–Pt Nanoparticles. ACS Catal. 2015, 5, 7, 3916-923.

59.   McCormac, T.; Cassidy, J.; Cameron, D. Electrochemical deposition of prussian blue films across interdigital array electrodes and their use in gas sensing. Electroanalysis. 1996, 195-198

60.   Weixin, L.; Zhang, R.; Pengran, G.; Lixu, L. Studies on the Faradaic Efficiency for Electrochemical Reduction of Carbon Dioxide to Formate on Tin Electrode. J. Power Sources. 2014, 253, 276-281.

61.   Reda, T.; Plugge, C. M.; Abram, N. J.; Hirst, J. Reversible interconversion of carbon dioxide and formate by an electroactive enzyme. Proc. Natl. Acad. Sci. 2008. 105, 31, 10654–10658.

62.   Bassegoda, A.; Madden, C.; Wakerley, D. W.; Reisner, E.; Hirst, J. Reversible Interconversion of CO_2 and Formate by a Molybdenum-Containing Formate Dehydrogenase. J. Am. Chem. Soc. 2014, 136, 44, 15473–15476.

VITA

SAMI ALHARBI

Education:	M. S. In Chemistry East Tennessee State University Johnson city, TN (August, 2019) B.S. in Chemistry Qassim University Qassim, Saudi Arabia (May, 2014)
Employment:	Teaching Assistant Buraydah College Qassim, Saudi Arabia Dentistry (Aug 2014-Dec 2014)
Teaching	Teaching Assistant Qassim University College of Science (Jan 2015 - present)
Presentation:	Sami Alharbi, *Dane W. Scott. Reproducible Electrodeposition of Hydrogen Molybdenum Bronze Films and Electrochemical Reduction of Carbon Dioxide at Low Over Potentials American Chemical Society, Augusta, GA,2018 (11/5/2018 poster presentation, SERMACS 2018)